THE JOURNAL OF PHYSICAL CHEMISTRY C

Article

pubs.acs.org/JPCC

Periodic Hybrid DFT Approach (Including Dispersion) to $MgCl_2$-Supported Ziegler–Natta Catalysts. 2. Model Electron Donor Adsorption on $MgCl_2$ Crystal Surfaces

Fabio Capone,[†] Luca Rongo,[†] Maddalena D'Amore,*[,†,§] Peter H. M. Budzelaar,[‡,§] and Vincenzo Busico[†,§]

[†]Dipartimento di Scienze Chimiche, Università di Napoli Federico II, Via Cintia, 80126 Napoli, Italy

[‡]Department of Chemistry, University of Manitoba, Winnipeg, MB R3T 2N2, Canada

[§]Dutch Polymer Institute (DPI), 5600 AX Eindhoven, The Netherlands

Supporting Information

ABSTRACT: The adsorption of small probe molecules (H_2O, NH_3 and EtOH) and the small model silane $Me_2Si(OMe)_2$ on (104) and (110) surfaces of α-$MgCl_2$ have been studied using periodic DFT calculations including a classical correction (of the type $f(R)/R^6$) for dispersion. The results reveal that donors strongly stabilize both crystal surfaces relative to the bulk solid. Moreover, coordination of two donor molecules to the four-coordinate exposed Mg atom of $MgCl_2$ (110) causes this surface to become preferred over $MgCl_2$ (104) surface with only a single donor per exposed Mg. However, coverage also plays an important role. The model silane preferentially adsorbs in bidentate mode on $MgCl_2$ (110), provided that coverage is 0.5 or lower; at full coverage, there is not enough space for such an arrangement, and only a monodentate binding mode is obtained. Such coverage effects should be even more pronounced for the bulkier silanes used as external donors in real $MgCl_2$-supported Ziegler–Natta systems, as tailored experiments seem to confirm.

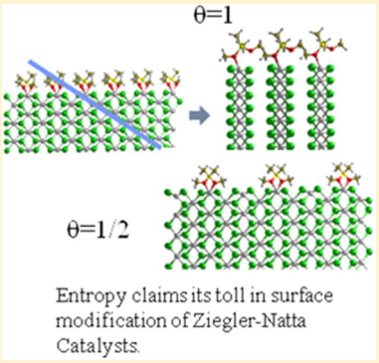

INTRODUCTION

With a global market of over 50 MT in 2012, the market share of isotactic polypropylene (iPP) among the largest-volume synthetic polymers continues to grow.[1] Notwithstanding the competition by molecular catalysts, classical $MgCl_2$-supported Ziegler–Natta systems (ZNS)[2,3] are still leading in iPP production technology.[4] These systems partly represent black-boxes from a mechanistic standpoint and are definitely far from perfection. The two facts together prompted us to launch an intensive research program revisiting the subject with an integrated state-of-the-art experimental and computational approach.

ZNS for iPP[2,3] feature a nanocrystalline $MgCl_2$ matrix, on which chiral Ti-based active species are generated from simple nonchiral precursors (typically, $TiCl_4$) by reaction with an Al-trialkyl (e.g., $AlEt_3$). Coadsorbed electron donors (mostly bidentate organic molecules like diesters, diethers, and dialkoxysilanes) tailor the local environment of the transition metal, enhancing the regio- and enantioselectivity at the propene insertion step very much like the ancillary ligand(s) of molecular catalysts, albeit in a far less defined context. In most cases, *pairs* of electron donors are used: one added to the solid precatalyst *during its synthesis* (internal donor, ID), another in combination with the AlR_3 (external donor, ED).[2,3] Exchange of ID and ED on the catalyst surface can occur under polymerization conditions in case the ID reacts with AlR_3;[5−7] this may explain the specificity observed in the composition of successful ID/ED donor pairs.[2,3]

$MgCl_2$ has a layer structure[8] similar to that of the violet modifications of $TiCl_3$[9] (the original catalyst family disclosed by Natta in the 1950s).[2] A long-standing hypothesis is that the epitaxial chemisorption of $TiCl_4$ on this matrix results into catalytically active surfaces mimicking authentic violet $TiCl_3$ ones.[2] In particular, according to seminal work by Corradini,[10] dinuclear Ti_2Cl_8 adducts on $MgCl_2$(100) lateral terminations (104 in α-$MgCl_2$, the stable crystal polymorph[8]) would be changed by the AlR_3 cocatalyst into Ti_2Cl_5R species with stereogenic and coordinatively unsaturated Ti centers (Figure 1), able to mediate propene polymerization in isotactic fashion. This interpretation, however, largely based on pioneering applications of molecular mechanics (MM),[10] turned out to be flawed as soon as quantum mechanics (QM) methods became able to address the problem. Parrinello was the first to conclude that the proposed Ti_2Cl_5R species on $MgCl_2$(100) [α-$MgCl_2$(104)] is unstable,[11−13] and Ziegler confirmed his finding.[14] The known fact that density functional theory (DFT) methods often do not adequately account for dispersive interactions, of fundamental importance in these structures, along with more technical difficulties associated with the description of atoms with highly polarizable electron clouds (e.g., Cl),[15] resulted into a confusing picture for quite some

Received: July 15, 2013
Revised: October 31, 2013
Published: October 31, 2013

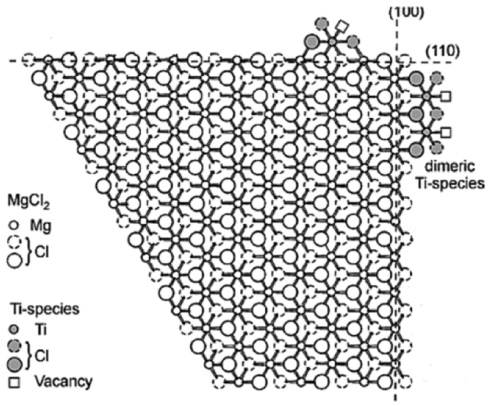

Figure 1. Epitaxial precursors of active Ti species on lateral α-$MgCl_2$ crystal terminations according to Corradini.[10] The dinuclear adduct on α-$MgCl_2$(104), in particular, would evolve into an isotactic-selective active species.

time, culminating with the puzzling claim that $MgCl_2$ would be tout court unable to bind $TiCl_4$.[14]

With state-of-the-art DFT calculations including a semi-empirical correction for dispersion (the so-called DFT-D approach), or by exploiting the latest-generation meta-GGA functionals explicitly developed for systems with long-range electron correlations (e.g., the M06 family), we ultimately concluded that possible docking sites for $TiCl_4$ are located primarily on $MgCl_2$(110), exposing 4-coordinated Mg atoms (Figure 2).[16] This is somewhat ironic, considering that such

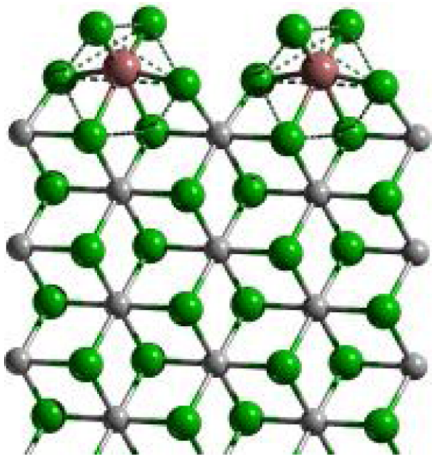

Figure 2. $TiCl_4$ adsorbed on $MgCl_2$(110).[16]

surfaces had long been claimed to be home to non-stereoselective catalytic species only,[10] and bidentate electron donors assumed to chelate to said doubly unsaturated Mg atoms and hinder $TiCl_4$ binding.[2,3,10,17−19] However, it is not difficult to construct models of isotactic-selective mononuclear $TiCl_2R$ catalytic species chemisorbed epitaxially on $MgCl_2$(110), be it that these require coadsorbed electron donor molecules close by, to tighten the chiral Ti pocket and ensure an effective selection of the propene insertion mode.[20,21] This conclusion is consistent with all available experimental results, including recent spectroscopic studies of precatalysts,[22,23] and active site fingerprinting analyses of polymer microstructure.[20,24]

An apparent contradiction is that, according to state-of-the-art DFT(-D) studies,[15,25] well-formed α-$MgCl_2$ crystals should only feature, in addition to basal (00l) planes, $MgCl_2$(104), and equivalent lateral terminations, exposing 5-coordinated Mg atoms; as a matter of fact, these are lower in energy than $MgCl_2$(110) terminations by ∼0.15 J m^{-2}. However, we[15,25] and others[26−28] noted that the relative stability of the two types of lateral terminations can be reversed by the interaction with adsorbates; this is one of the two focal points of the present article. The other is the key effect of surface coverage in determining the adsorption mode of electron donors, from small probe molecules like ethanol to larger bidentate moieties of industrial interest such as dialkoxysilanes.

In the next sections, we will elaborate in detail on both aspects. We restricted our computational analysis to α-$MgCl_2$ crystals with ideal 2-D periodicity and well-formed (104) and (110) surfaces. Real primary particles in ZNS are nano-sized,[2,3,15] and therefore, the presence of defects (e.g., edges, steps, corners, etc.) is very significant.[29] In concluding this introduction, we find it worthy to note that, like all chemical processes, chemisorption is driven by free energy, and therefore, any calculations aimed to predict surface equilibria should produce ΔG_{ads} values. However, in the previous literature this is an exception rather than the norm.[30] Calculating entropy contributions for surface-adsorbed species is not trivial, but the computational codes we adopted include them at state-of-the-art level.

METHODS SECTION

Computational Details. The DFT-D approach to molecular adsorption on $MgCl_2$ surfaces closely followed our earlier work.[16]

Concerning the slab thickness, we adopted the one needed for convergence, that is approaching bulk-like behavior in the middle of the slab; this turned out to lie in the range of about 1.8 to 3.0 nm (depending on the spacing between the *hkl* lattice planes considered). As for the computation constraints, starting from the fully optimized bulk α-$MgCl_2$, slab models were cut, molecules were adsorbed on the thus generated surfaces, and internal coordinates of both adsorbates and $MgCl_2$ surfaces were fully relaxed keeping the cell parameters fixed.

All calculations were performed using the CRYSTAL09 periodic code.[31] Geometries were computed at the B3LYP-D2[32,33] level (the modification proposed by Civalleri and co-workers to Grimme's standard set of parameters was adopted),[34] with the following all-electron basis sets: triple-ζ plus polarization (TZVP) quality for Mg, Ti, and Cl atoms[16] and an Ahlrichs VTZ[35] plus polarization quality for the adsorbed molecules. In the latter case, a preliminary study was carried out to optimize the coefficients of the polarization Gaussian functions, thus enabling more accurate calculations of adsorption energy and vibrational frequencies. To check the quality of our predictions, the BSSE (basis set superposition error) was computed with the counterpoise method,[36] and found to be ∼10% of the total adsorption energy; this is an indication that the customized Ahlrichs VTZ plus polarization basis sets were adequate, and the vibrational analyses were not basis-set-biased.

All ΔE_{ads} values are given in kJ per mol of adsorbate (regardless of adsorbate binding mode), using fully relaxed unit cells for bare and covered crystals, and also in J m^{-2} for reasons that will be explained in a following section. Vibrational analysis was carried out under standard conditions (p = 1 bar, T = 298

dx.doi.org/10.1021/jp406977h | J. Phys. Chem. C 2013, 117, 24345−24353

Table 1. Values of ΔE_{ads}, $T\Delta S_{ads}$, and ΔG_{ads} under Standard Conditions, Calculated at B3LYP-(D2)/TZVP, VTZp Ahlrichs Level, for Three Electron Donor Probes on α-$MgCl_2$(104) and α-$MgCl_2$(110)

entry	donor	surface (*hkl*)	ϑ	R	ΔE_{ads} (kJ mol^{-1})	ΔE_s (J m^{-2})	$-T\Delta S_{ads}$ (kJ mol^{-1})	ΔG_{ads} (kJ mol^{-1})
1	(none)	104	1	1		0.276		
2		110	1	1		0.399		
3	H_2O	104	1	1	−86.6	−0.267	41.3	−36.4
4		110	1	1	−126.8	−0.174	44.3	−74.1
5		110	1	2	−110.8	−0.602	42.6	−59.7
6	NH_3	104	1	1	−90.5	−0.292	41.9	−39.5
7		110	1	1	−135.9	−0.215	45.0	−81.2
8		110	1	2	−113.3	−0.625	46.1	−57.8
9	EtOH	104	1	1	−79.3	−0.221 (0.027)[a]	46.5	−23.7
10		110	1	1	−116.1	−0.126 (0.053)[a]	47.6	−60.5
11		110	1	2	−86.7	−0.384 (−0.027)[a]	56.8	−20.0

[a]Values in parentheses are relative to liquid EtOH.

K) to calculate ΔS_{ads} and hence the Gibbs free energy of adsorption ΔG_{ads}. Periodic DFT-based methods have only recently been used to perform vibrational analysis of crystalline solids. Most periodic codes are based on plane-wave basis sets in combination with pseudopotentials; using such basis sets makes it difficult to include the Hartree−Fock exchange term needed in hybrid functionals (such as B3LYP). The CRYSTAL09 code, however, employs Gaussian-type local basis sets; this allowed a smooth implementation of B3LYP, a functional of proven reliability in computing vibrational properties.[37−39] The vibrational analysis protocol used here is similar to the computational scheme of many molecular codes, using analytical gradients of the energy with respect to nuclear positions and numeric differentiation to obtain the Hessian at the central point of the first Brillouin zone (Γ point, point $k = 0$ in BZ). A drawback of our choice of functional is that B3LYP has been found to end up with (much) lower adsorption and complexation energies than a number of other functionals;[40] this affects their absolute values, which therefore should be taken with caution, but not the general conclusions of our study.

Experimental Details. ID/ED exchange experiments were carried out on a typical $MgCl_2$/$TiCl_4$/dibutylphthalate (DBP) precatalyst sample[2] (donated by Sabic), containing 2.7 wt % of Ti (metal) and 16.3 wt % of DBP. The sample was characterized by X-ray powder diffraction on a Philips PW 1830 setup equipped with a custom-made airtight cell with PVC windows, able to maintain a static atmosphere with negligible O_2 and moisture contamination for at least 8 h. The cell was loaded in an MBraun LabMaster 130 glovebox under Argon (water and oxygen levels <1 ppm_v) and transferred to the diffractometer, where the diffraction profile was collected using Ni-filtered CuK_α radiation (20 mA, 40 KV) with a step-scanning procedure (2θ range between 5° and 70°, 0.1° step, 30 s counting time per step). The average dimensions of the $MgCl_2$ crystallites were estimated from the 003 and 110 diffraction peaks according to the method of Allegra and Giunchi.[41]

All experiments were carried out at least in duplicate in a Freeslate Extended Core Module (XCM) robotic platform equipped with a dual-arm robot, bearing a vial gripper and a solid dispenser (right arm), and dedicated handling lines and needles for solutions (right arm) and slurries (left arm). The platform was integrally contained in a triple MBraun LabMaster glovebox, maintaining a N_2 atmosphere with water and oxygen levels below 0.1 ppm_v. Heptane suspensions of the precatalyst were treated at 70 °C for 30 min with $AlEt_3$/$Me_2Si(OEt)_2$ or $AlEt_3$/$^{iso}Bu_2Si(OMe)_2$ mixtures, or with $^{iso}Bu_2Si(OMe)_2$ alone, at variable [Si]/[Ti] molar ratio (in the 0−15 range), and [Al]/[Ti] = 25 (when used). A further set of experiments was performed at [Si]/[Ti] = 2.5 and [Al]/[Ti] = 25, changing the reaction time between 5 and 30 min. After the reaction, the solid phases were washed twice with heptane at 25 or 70 °C, then with pentane, and dried in a Savant SPD121P centrifugal drying station at 45 °C for 3 h at 1400 rpm under vacuum (1.0×10^3 Pa). The detailed reaction protocol is provided as Supporting Information.

Aliquots of the dry samples were then dissolved in methanol-d_4 inside 5 mm NMR tubes, taken out of the glovebox, and analyzed by ^{1}H NMR to quantify the residual DBP and the chemisorbed dialkoxysilane. Quantitative ^{1}H NMR spectra were recorded with a Bruker Avance DRX 400 spectrometer operating at 400 MHz. Acquisition conditions were 5 mm probe; acquisition time, 3.0 s; relaxation delay, 5.0 s; pulse angle, 90°; spectral width, 10 ppm; 100 transients. Peak assignment was based on the literature and preliminary ^{1}H NMR characterizations of the investigated donor molecules. Quantitative determinations were based on peak integrations against that of an aliquot of acetonitrile (10 μL) added as internal standard (methyl peak at $\delta = 2.05$ ppm downfield of TMS). In the case of DBP, we chose to integrate the aromatic protons in the $\delta = 7.0$−8.0 ppm range, so as to cover all reduction products of DBP with $AlEt_3$ possibly coadsorbed with unreacted DBP.

RESULTS AND DISCUSSION

Computational Study. In this section, we report and discuss the calculated values of adsorption energy (ΔE_{ads}) and standard free energy (ΔG_{ads}) for the investigated adsorbates on α-$MgCl_2$(104) and α-$MgCl_2$(110), for various degrees of fractional coverage (θ) and molar ratios (R) between adsorbate and exposed substrate Mg sites. We define θ as the fraction of total exposed Mg atoms on the considered surface involved in chemisorption; there is no necessary relationship between θ and R because in some cases more than one molecule can adsorb on the same Mg, whereas in others one single molecule can occupy two Mg adsorption sites. One should also realize that some adsorbates are too bulky to end up with a full surface coverage. In view of all this, for each optimized surface/adsorbate structure the DFT-D adsorption energy ΔE_{ads} is given in kJ mol(adsorbate)$^{-1}$; in addition, the surface energy ΔE_s (in J m^{-2}) is also provided, to facilitate semiquantitative

dx.doi.org/10.1021/jp406977h | J. Phys. Chem. C 2013, 117, 24345−24353

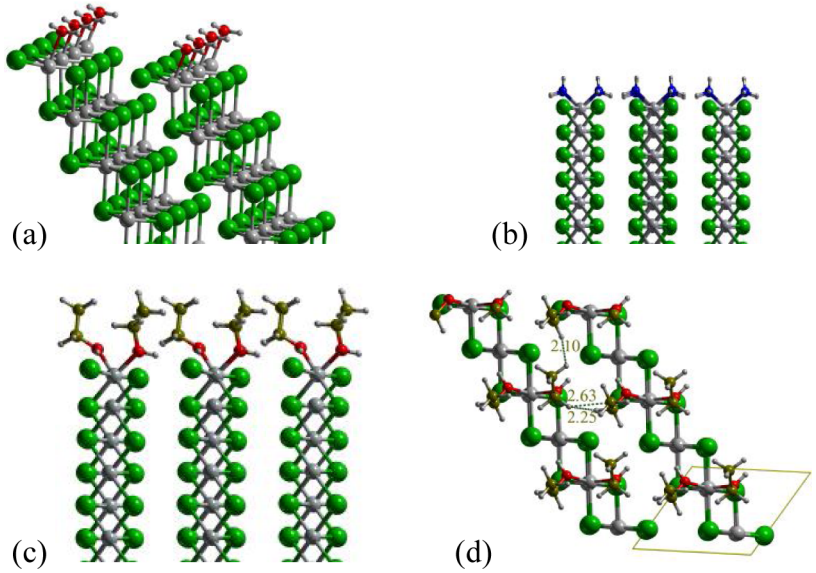

Figure 3. Small donor molecules adsorbed on α-$MgCl_2$: (a) H_2O on $MgCl_2(104)$, (b) 2 NH_3 per Mg on $MgCl_2(110)$, (c) 2 EtOH per Mg on $MgCl_2(110)$, (d) 2 EtOH per Mg on $MgCl_2(110)$. Panels a–c are side views,; panel d is a top view.

comparisons of relative crystal surface stabilities. (ΔE_s was computed as the sum of the surface energy (in J m^{-2}) (that is the energy of formation of a certain surface starting from the bulk) and the $\Delta E_{ads}/A$ (in J m^{-2}) for the adsorption of each molecule on the considered surface.)

Three small electron donor probe molecules, namely, H_2O, NH_3 and EtOH, were chosen for a first set of 2-D periodic DFT-D calculations. Water is ubiquitous and always present in formally neat $MgCl_2$ samples. Ammonia is a common probe for adsorption studies, and in the present case, it can be viewed as the prototype of N-EDs (e.g., amines). EtOH, in turn, is relevant because for many industrial ZNS the $MgCl_2$ support is made through loss of EtOH from $MgCl_2 \cdot n$EtOH adducts ($1 < n < 3$).[2,3,42,43] The results are summarized in Table 1, whereas Figure 3 shows some relevant optimized structures.

All three probe molecules are predicted to chemisorb on $MgCl_2$ with rather similar energies. We calculate $\Delta E_{ads} \approx -80$ to -90 kJ mol^{-1} for binding to a 5-coordinated Mg site on $MgCl_2(104)$, and $\Delta E_{ads} \approx -115$ to -135 kJ mol^{-1} for binding a *first* molecule to a 4-coordinated Mg on $MgCl_2(110)$; this is about 50% larger than in the former case. For all probe molecules, the calculated values of surface energy E_s are negative, meaning that breaking up the bulk and forming either (104) or (110) surfaces is favorable in the presence of these donors; as a matter of fact, H_2O and EtOH are good solvents for $MgCl_2$. The difference between adsorption on $MgCl_2(104)$ and *single* adsorption on $MgCl_2(110)$ is not large enough to overcome the intrinsic preference for formation of $MgCl_2(104)$: E_s is -0.22 to -0.29 J m^{-2} for $MgCl_2(104)$ vs -0.13 to -0.22 J m^{-2} for $MgCl_2(110)$. However, binding a *second* molecule to a 4-coordinated Mg changes the picture and in all cases makes $MgCl_2(110)$ the preferred exposed surface. With H_2O and NH_3, the calculated binding of the second donor to $MgCl_2(110)$ (~ -110 kJ mol^{-1}) is only slightly weaker than for the first donor and still stronger than that to a 5-coordinated Mg on $MgCl_2(104)$. Steric crowding, however, starts to show up for the comparatively bulkier EtOH molecule, leading to a larger energy drop between the first and second binding ($\sim$30 vs $\sim$20 kJ mol^{-1}; compare entries 10/11 with entries 4/5 and 7/8 of Table 1). It should be noted that the hindrance is not so much between the two EtOH molecules at each given Mg center but rather with those at neighboring surface sites (Figure 3c,d).

The loss of rotational and translation degrees of freedom of the adsorbate typically contributes $-T\Delta S_{ads} \approx 40-50$ kJ mol^{-1} to the adsorption free energy for a gas-phase molecule at room temperature, somewhat less ($\sim$25–35 kJ mol^{-1}) in the liquid phase.[44,45] Our calculated values for the entropic contributions of binding (gaseous) H_2O and NH_3 in all examined cases and a *single* EtOH molecule to a Mg site on $MgCl_2(104)$ or $MgCl_2(110)$ are consistent with this. However, the entropic contribution of binding a *second* EtOH molecule to $MgCl_2(110)$ turns out to be somewhat larger (by about 10 kJ mol^{-1}; entry 11 of Table 1), which likely indicates that in the bis(ethanol) adduct molecules are more rigidly constrained due to the tight packing and have also lost some of their *vibrational* freedom.

Next, we examined the case of an industrially relevant ED class, i.e., dialkyldialkoxysilanes.[2,3] For our computational study, we identified $Me_2Si(OMe)_2$ as a minimal model of the bulkier molecules of choice in the industrial practice [like $^{iso}Bu_2Si(OMe)_2$]. Many literature studies have covered dialkoxysilane chemisorption on $MgCl_2$;[30] the most common assumption is that the interaction with the surface is through both O atoms, either in chelate mode to one single 4-coordinated Mg center on $MgCl_2(110)$ or equivalent surfaces (Figure 4a), or in the so-called bridge mode to two adjacent 5-coordinated Mg centers on $MgCl_2(104)$ or equivalent surfaces (Figure 4b). In the latter case, though, the Mg···Mg distance of 3.698 Å constrains the

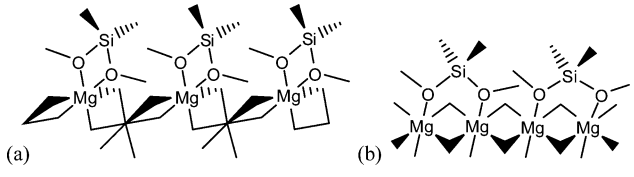

Figure 4. Proposed structures for dialkoxysilanes adsorbed on α-$MgCl_2$: (a) chelate on $MgCl_2(110)$; (b) bridge on $MgCl_2(104)$.

dx.doi.org/10.1021/jp406977h | J. Phys. Chem. C 2013, 117, 24345–24353

Table 2. Values of ΔE_{ads}, $T\Delta S_{ads}$, and ΔG_{ads} under Standard Conditions, Calculated at B3LYP-(D2)/TZVP, VTZp Ahlrichs Level, for $Me_2Si(OMe)_2$ on α-$MgCl_2(104)$ and α-$MgCl_2(110)$ in Different Binding Modes

entry	surface/binding mode	ϑ	R	ΔE_{ads} (kJ mol^{-1})	E_s (J m^{-2})	$-T\Delta S_{ads}$ (kJ mol^{-1})	ΔG_{ads} (kJ mol^{-1})
1	$MgCl_2(104)$/bridge	1	1/2	−110.0	−0.069	76.1	−13.7
2	$MgCl_2(110)$/monodentate	1	1	−108.7	−0.092	64.2	−29.5
3	$MgCl_2(110)$/chelate	1/2	1/2	−155.8	0.047	59.1	−79.0

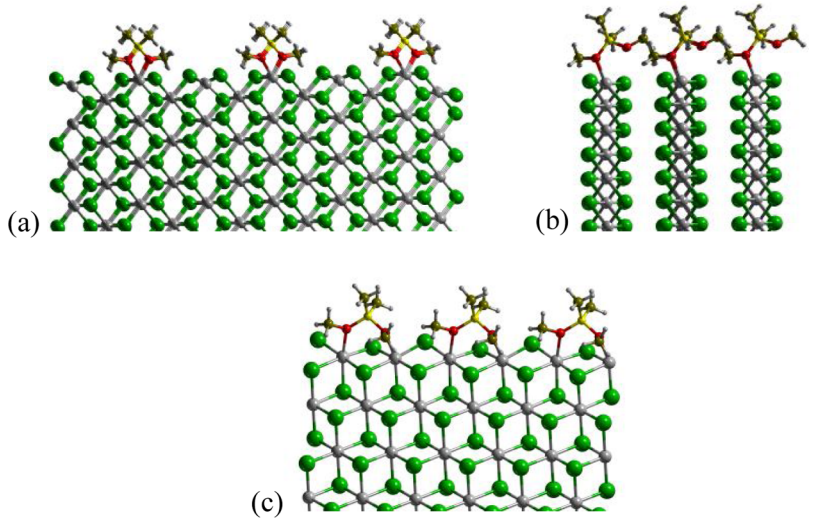

Figure 5. $Me_2Si(OMe)_2$ adsorbed on α-$MgCl_2$: (a) chelate on $MgCl_2(110)$, ϑ = 1/2; (b) monodentate on $MgCl_2(110)$, ϑ = 1; (c) bridge on $MgCl_2(104)$, ϑ = 1.

adsorbate into a highly stretched conformation, which makes the binding less effective.

Our DFT-D results are summarized in Table 2; optimized structures are shown in Figure 5. The model silane did actually bind to the $MgCl_2(104)$ surface in the aforementioned bridge mode (entry 1 of Table 2 and Figure 5a), but the calculated adsorption energy (ΔE_{ads} = −110 kJ mol^{-1}) was close to that of a *monodentate* probe molecule (entries 3, 6, and 9 of Table 1); this is a sign that much of the additional binding energy provided by the second Mg−O bond was counterbalanced by the strain associated with accommodating the bridge geometry. In addition, we find a large positive entropy contribution to the standard adsorption free energy ($-T\Delta S_{ads}$ = 76 kJ mol^{-1}), which may in part be due to the bidentate binding mode (loss of flexibility), and in part to interactions with neighboring adsorbates (similarly to the $MgCl_2(110)$/bis(EtOH) adduct discussed above). The calculated final free energy of adsorption (ΔG_{ads} = −14 kJ mol^{-1}) is so low that binding can at best be called weak, and a silane bound this way would presumably be washed away quite easily. If said value is realistic (see our remark on absolute ΔE_{ads} values in the Computational Details section, though), then the considered interaction is *not* likely to be important for catalysis, even though it was originally claimed as one of the design features of alkoxysilane EDs.[2,30] Experimental results in this article (vide infra) and previous high-resolution magic-angle-spinning (HR-MAS) ^{1}H NMR data[15] are actually in line with such a conclusion.

For adsorption on $MgCl_2(110)$, we ruled out a priori the hypothesis of a bridge interaction, in view of the even larger Mg···Mg distance on this surface (6.405 Å) compared with $MgCl_2(104)$, and started our analysis with the commonly accepted chelate binding mode. At full coverage (θ = 1), the geometry spontaneously evolved into a monodentate mode (entry 2 of Table 2 and Figure 5b) because steric interference between first neighbors forced the molecules to adopt a slimmer arrangement. The calculated binding energy of ΔE_{ads} = −109 kJ mol^{-1} is slightly lower than that of single small probe donors on the same surface (entries 2, 5, and 8 of Table 1); the entropic contribution ($-T\Delta S_{ads}$ = 65 kJ mol^{-1}), in turn, suggests strong internal motion restrictions even in this mode, and therefore, the computed value of ΔG_{ads} = −29.5 kJ mol^{-1} is, again, indicative of a relatively weak binding. Reducing the coverage to θ = 1/2, however, relieves steric pressure considerably; the adsorbate stayed bidentate (Figure 5a), and ΔE_{ads} increased by about 50% relative to full coverage (entry 3 of Table 2). Taking the entropic term into account, it appears that the steric relief at θ = 1/2 more than compensates for the constraints imposed by chelation, and the calculated ΔG_{ads} = −155.8 kJ mol^{-1} is indeed much lower than for θ = 1 (compare entries 2 and 3 of Table 2). However, the calculated surface energy for θ = 1/2 (0.047 J m^{-2}) remains less favorable than for θ = 1 (−0.092 J m^{-2}) since the stronger silane binding at low coverage is counterbalanced by the lower number of adsorbate molecules bound per surface area. In any case, considering that alkoxysilane EDs of industrial use are much bulkier than the one investigated here, the only possible conclusion is that complete saturation of all Mg sites in real catalysts by these molecules is unfeasible. We will comment on the implications for catalysis in the Conclusions.

These results about the influence of surface coverage on the coordination capability of silane donor molecules, in particular on $MgCl_2(110)$, are in fairly good agreement with those reported in a recent DFT study not including the dispersion contribution in the evaluation of the adsorption energy;[46] on the contrary, any comparisons of our free energies data are not possible since to the best of our knowledge the present article is the first to provide such values for these complex systems.

dx.doi.org/10.1021/jp406977h | J. Phys. Chem. C 2013, 117, 24345−24353

Experimental Study. In this part, we report experimental data on the adsorption of dialkyldialkoxysilane molecules on real ZNS surfaces, for comparison with calculated ones. The seemingly logical choice of using model samples of neat, activated $MgCl_2$ was ruled out because, based on the data in Table 1 on water adsorption, simple calculations making use of the Langmuir isotherm indicated that naked $MgCl_2$ surfaces are inevitably contaminated even when rapidly handled in a glovebox environment. In agreement with this conclusion, for physically activated $MgCl_2$ samples with average primary particle sizes of the order of 100−150 nm, we typically measured water contents in the 0.3−0.5 wt % range. In view of the above, for our experimental studies of silane adsorption we opted for a sample of $MgCl_2/TiCl_4$/DBP (DBP = dibutylphthalate) precatalyst, in which the lateral terminations of the primary particles are protected by chemisorbed $TiCl_4$ and DBP molecules; as is well-known, DBP can then be removed in a controlled way by reaction with the Al-alkyl cocatalyst.[2,3] According to powder X-ray diffraction data, the average crystallite size in the investigated precatalyst sample was ∼8 nm in the basal planes, and ∼2 nm perpendicular to them, which is typical of industrial precatalysts.[2,3] From the thus determined basal plane dimensions, in particular, corresponding to ∼20 unit cells along the side edges of structural layers, one can estimate a fraction of exposed Mg atoms in the sample of ∼15−20%; the DBP and $TiCl_4$ contents of 7.9 and 7.5 mol % relative to Mg, respectively, are consistent with a very high surface area and indicate a high cumulative surface coverage.

The sample was then reacted with $AlEt_3$ in the presence of two dialkoxysilanes of different steric bulk, namely, $Me_2Si(OEt)_2$ and $^{iso}Bu_2Si(OMe)_2$, to liberate the surface part covered by DBP and let the silane take its place.[2,3,6] Sets of experiments for systems of composition $MgCl_2/TiCl_4$/DBP + $AlEt_3/R_2Si(OR')_2$ and, for comparative purposes, $MgCl_2/TiCl_4$/DBP + $^{iso}Bu_2Si(OMe)_2$ were carried out with the results of Tables 3 and 4 and Figures 6 and 7.

The data clearly indicate that under the used conditions, which are reasonably close to those experienced by the solid particles in catalysis, (a) ID/ED exchange was extensive and rather fast (less than 5 min; Figure 6), (b) DBP displacement was entirely due to reaction with $AlEt_3$ (Table 4), and (c) the alkoxysilane could only chemisorb once free $MgCl_2$ surface had become available in consequence to the previous process (compare Tables 3 and 4). As a matter of fact, exposing the precatalyst to $^{iso}Bu_2Si(OMe)_2$ alone did not lead to any appreciable release of DBP, and the very modest amounts of adsorbed silane were only weakly bound and could be washed out completely at 70 °C (Table 4).

Notably, in the two investigated $MgCl_2/TiCl_4$/DBP + $AlEt_3/R_2Si(OR')_2$ systems, despite a very different steric demand the

Table 3. Amounts of DBP and $R_2Si(OR')_2$ in the Solid Phases Recovered after Reacting $MgCl_2/TiCl_4$/DBP with $AlEt_3/R_2Si(OR')_2$ in Heptane Slurry at 70°C for 30 min ([Al]/[Ti] = 25; for Details, See Experimental Details)

entry	system	[Si]/[Ti]	ID	ED[a]	total donor[a]
1	$MgCl_2/TiCl_4$/DBP + $AlEt_3/Me_2Si(OEt)_2$	1.25	1.4	5.3	6.7
2		2.50	1.4	4.7	6.1
3		6.25	1.3	7.2	8.5
4		10.0	1.9	7.9	9.8
5		12.5	1.7	8.7	10.4
6		15.0	1.6	9.0	10.6
7	$MgCl_2/TiCl_4$/DBP + $AlEt_3/^{iso}Bu_2Si(OMe)_2$	1.25	1.4	3.3	4.7
8		2.50	2.1	5.7	7.8
9		6.25	1.9	7.1	9.0
10		10.0	1.2	7.6	8.8
11		12.5	1.1	8.3	9.4
12		15.0	1.7	7.5	9.2

[a]mol % wt Mg.

Table 4. Amounts of DBP and $^{iso}Bu_2Si(OMe)_2$ in the Solid Phases Recovered after Reacting $MgCl_2/TiCl_4$/DBP with $^{iso}Bu_2Si(OMe)_2$ or $AlEt_3/^{iso}Bu_2Si(OMe)_2$ in Heptane Slurry at 70°C for 30 min, Followed by Washing at 25 or 70°C ([Al]/[Ti] = 25; for Details, See Experimental Details)

				$^{iso}Bu_2Si(OMe)_2$[a]	
entry	system	[Si]/[Ti]	DBP[a]	washing at 25 °C	washing at 70 °C
1	$MgCl_2/TiCl_4$/DBP + $^{iso}Bu_2Si(OMe)_2$	1.25	8.2	1.2	0.1
2		6.25	9.0	1.7	0.1
3		13.0	8.3	0.8	0.3
4	$MgCl_2/TiCl_4$/DBP + $AlEt_3/^{iso}Bu_2Si(OMe)_2$	1.25	1.4	7.7	4.2
5		2.50	2.1	5.7	5.8
6		6.25	1.9	6.8	6.4

[a]mol % wt Mg.

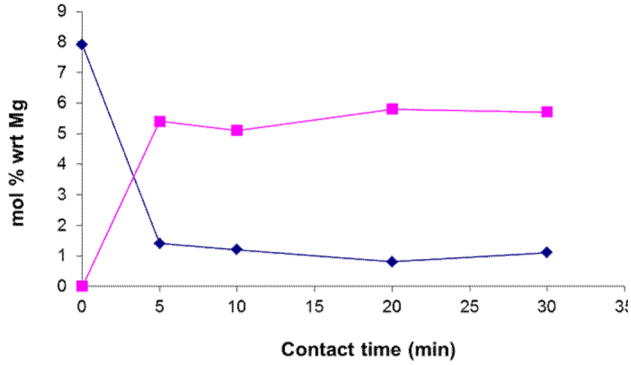

Figure 6. Kinetics of DBP/$^{iso}Bu_2Si(OMe)_2$ exchange for $MgCl_2/TiCl_4$/DBP + $AlEt_3/^{iso}Bu_2Si(OMe)_2$ in heptane slurry at 70 °C ([Al]/[Ti] = 25; [Si]/[Ti] = 2.5). ♦ = DBP; ■ = $^{iso}Bu_2Si(OMe)_2$ in the solid phase (as measured by ^{1}H NMR).

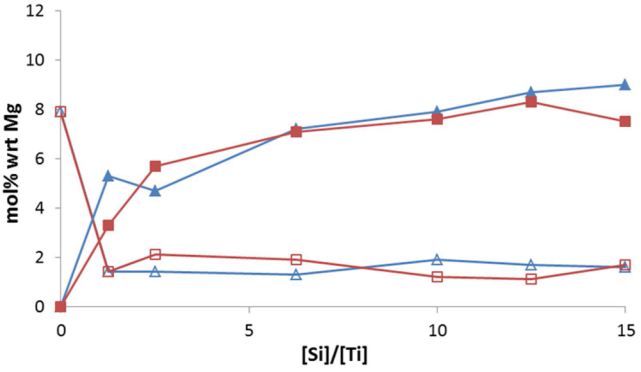

Figure 7. Results of DBP/$R_2Si(OR')_2$ exchange for $MgCl_2/TiCl_4$/DBP + $AlEt_3/^{iso}Bu_2Si(OMe)_2$ and $MgCl_2/TiCl_4$/DBP + $AlEt_3/(Me)_2Si(OEt)_2$, reacted in heptane slurry at 70 °C for 30 min. □,△ = DBP; ■ = $^{iso}Bu_2Si(OMe)_2$; ▲ = $Me_2Si(OEt)_2$ in the solid phase (as measured by ^{1}H NMR).

dx.doi.org/10.1021/jp406977h | J. Phys. Chem. C 2013, 117, 24345−24353

two dialkoxysilanes chemisorbed in practically identical molar amounts, reaching the same surface saturation value within the experimental error (Table 3 and Figure 7). A plausible explanation for this finding is that chemisorption occurred at the surface vacancies created by DBP removal and that these are unable to accommodate more than 1 molecule of alkoxysilane per molecule of DBP despite the smaller size of $Me_2Si(OEt)_2$ compared to $^{iso}Bu_2Si(OMe)_2$; of course, this would correspond to a higher surface area occupation in the latter case. Another educated guess is that both DBP and the alkoxysilanes were mainly bound on $MgCl_2(110)$ because the fairly strong alkoxysilane chemisorption (resistant to hot-washing) suggests a chelate adsorption mode (Figure 5a). If this interpretation is correct, the currently accepted models of catalytic species with ED molecules at nonbonded contact with the active sites[20] predict a different stereoselectivity in the two cases; indeed, the looser coverage of $MgCl_2(110)/TiCl_4/Me_2Si(OEt)_2$ should end up with a less effective steric modification of the active Ti species by the ED compared with $MgCl_2(110)/TiCl_4/^{iso}Bu_2Si(OEt)_2$ edges. As a matter of fact, polypropylene samples produced with $MgCl_2/TiCl_4/DBP - AlEt_3/Me_2Si(OEt)_2$ and $MgCl_2/TiCl_4/DBP - AlEt_3/^{iso}Bu_2Si(OMe)_2$ turned out to be moderately isotactic and highly isotactic, respectively.

CONCLUSIONS

In agreement with previous papers of this series,[15,16] the new computational and experimental results presented here confirm that $MgCl_2(110)$ (or equivalent) terminations with tetra-coordinated Mg are the most likely ZNS catalytic surfaces; as a matter of fact, these seem to be the only ones in $MgCl_2$ crystallites able to bind both $TiCl_4$ and dialkyldialkoxysilane EDs strong enough to hold them under precatalyst activation and polymerization conditions. As already noted, this conclusion represents a step change with respect to long-standing models pointing instead to $MgCl_2(104)$ (or equivalent) terminations with penta-coordinated Mg as the preferred surfaces for $TiCl_4$ chemisorption.[2,3,10,17] The latter surfaces are indeed the most plausible in *neat* $MgCl_2$ crystals,[15,25] but their lower Lewis acidity compared with $MgCl_2(110)$ favors the latter when adsorbates come into play.[15,25,28]

An important point highlighted by our DFT-D investigation is the strong steric interference between adjacent adsorbate molecules that builds up as soon as the degree of surface coverage becomes significant. This can be observed already with small probe donors (e.g., ethanol) but, understandably, is much more important with the bulky electron donors of industrial relevance; with alkoxysilane EDs, in particular, the situation of Figure 5a can be viewed as an upper limit before steric repulsion sets in. This fact may explain why a rather weakly interacting moiety like $TiCl_4$[16] can compete with much stronger donors like, e.g., diesters; indeed, one can imagine that the small $TiCl_4$ molecules fill the vacancies left on the surface by the large ID ones.[21,47] The precatalyst preparation protocols are consistent with this interpretation; as a matter of fact, in typical cases the $MgCl_2$ support is formed in the presence of strong electron donors (which should be functional to develop in preference $MgCl_2(110)$-type terminations), and $TiCl_4$ is always added at high temperature and in large excess with respect to the ID,[2] that is under conditions favoring local entropy-assisted reconstructions. One can imagine that, depending on the specific composition of the system, the exact structure of the resulting adducts is crucially dependent on the details of the procedure, and therefore the identification of the best conditions requires a careful and thorough exploration of the complex reaction variable hyperspace. Perusal of the examples reported in the patent literature[2] seems to confirm such a guess; an intriguing question then is to what extent the search was truly exhaustive in the investigated cases.

In a forthcoming paper, we will discuss phthalate IDs, which are even bulkier than the alkoxysilane EDs considered here and as such able to put steric pressure *between* adjacent $MgCl_2$ structural layers, rather than mainly *along the edges of individual layers*. As we shall see, this can have profound consequences on the average size and morphology of the primary precatalyst particles (making it necessary, inter alia, to adopt a different computational modeling approach).

ASSOCIATED CONTENT

Supporting Information

Full details of all experimental protocols and fractional coordinates for geometries of energy minima, for all computational models. This material is available free of charge via the Internet at http://pubs.acs.org.

AUTHOR INFORMATION

Corresponding Author

*(M.D.) E-mail: mdamore@unina.it. Tel: +39081674361.

Notes

The authors declare no competing financial interest.

ACKNOWLEDGMENTS

This work is part of the Research Program of the Dutch Polymer Institute (DPI), Eindhoven, The Netherlands, Project #712.

REFERENCES

(1) Jansz, J. Presentation at Fifth Annual India Chemical Industry Outlook Conference in Mumbai, 2012.www.chemweek.com/Assets/Session3_EBB_Jansz.pdf.

(2) Cecchin, G.; Morini, G; Piemontesi, F. In *Encyclopedia of Chemical Technology*; John Wiley and Sons:: New York, 2006; Vol. *26*, pp 502−554.

(3) Moore, E. P., Jr., Ed. *Polypropylene Handbook: Polymerization, Characterization, Properties, Applications*; Hanser Publishers:: Munich, Germany, 1996.

(4) Tullo, A. H. Metallocenes rise again. *Chem. Eng. News* **2010**, *88*, 10−16.

(5) Busico, V.; Corradini, P.; De Martino, L.; Proto, A.; Savino, V.; Albizzati, E. Polymerization of Propene in the Presence of Magnesium Cloride-Supported Ziegler−Natta Catalysts, 1. The Role of Ethyl Benzoate as "Internal" and "External" Base. *Makromol. Chem.* **1985**, *186*, 1279−1288.

(6) Busico, V.; Corradini, P.; De Martino, L.; Graziano, F.; Iadicicco, A. Propene Polymerization in the Presence of Magnesium Chloride-Supported Ziegler−Natta Catalysts, 4. Effects of Lewis Bases on Polymer Stereochemistry. *Makromol. Chem.* **1991**, *192*, 49−57.

(7) Noristi, L.; Barbè, P. C.; Baruzzi, G. Effect of the Internal/External Donor Pair in High-Yield Catalysts for Propylene Polymerization. 1. Catalyst−Cocatalyst Interactions. *Makromol. Chem.* **1991**, *192*, 1115−1127.

(8) Partin, D. E.; O'Keeffe, M. The Structures and Crystal Chemistry of Magnesium Chloride and Cadmium Chloride. *J. Solid State Chem.* **1991**, *95*, 176−183.

(9) Natta, G.; Corradini, P.; Allegra, G. The Different Crystalline Modifications of $TiCl_3$, a Catalyst Component for the Polymerization

of α-olefins. I. α-, β-, γ-$TiCl_3$. II. δ-$TiCl_3$. *J. Polym. Sci.* **1961**, *51*, 399−410.
(10) Corradini, P.; Barone, V.; Fusco, R.; Guerra, G. A Possible Model of Catalytic Sites for the Stereospecific Polymerization of α-Olefins on First-Generation and Supported Ziegler−Natta Catalysts. *Gazz. Chim. Ital.* **1983**, *113*, 601−607.
(11) Boero, M.; Parrinello, M.; Terakura, K. First Principles Molecular Dynamics Study of Ziegler−Natta Heterogeneous Catalysis. *J. Am. Chem. Soc.* **1998**, *120*, 2746−2752.
(12) Boero, M.; Parrinello, M.; Hüffer, S.; Weiss, H. First Principles Study of Propene Polymerization in Ziegler−Natta Heterogeneous Catalysis. *J. Am. Chem. Soc.* **2000**, *122*, 501−509.
(13) Boero, M.; Parrinello, M.; Weiss, H.; Hüffer, S. A First Principles Exploration of a Variety of Active Surfaces and Catalytic Sites in Ziegler−Natta Heterogeneous Catalysis. *J. Phys. Chem. A* **2001**, *105*, 5096−5105.
(14) Seth, M.; Margl, P. M.; Ziegler, T. A Density Functional Embedded Cluster Study of Proposed Active Sites in Heterogeneous Ziegler−Natta Catalysts. *Macromolecules* **2002**, *35*, 7815−7829.
(15) Busico, V.; Causà, M.; Cipullo, R.; Credendino, R.; Cutillo, F.; Friederichs, N.; Lamanna, R.; Segre, A.; Van Axel Castelli, V. Periodic DFT and High-Resolution Magic-Angle-Spinning (HR-MAS) ^{1}H NMR Investigation of the Active Surfaces of $MgCl_2$-Supported Ziegler−Natta Catalysts. The $MgCl_2$ Matrix. *J. Phys. Chem. C* **2008**, *112*, 1081−1089.
(16) D'Amore, M.; Credendino, R.; Budzelaar, P. H. M.; Causá, M.; Busico, V. A Periodic Hybrid DFT Approach (Including Dispersion) to $MgCl_2$-Supported Ziegler−Natta Catalysts. 1: $TiCl_4$ Adsorption on $MgCl_2$ Crystal Surfaces. *J. Catal.* **2012**, *286*, 103−110.
(17) Albizzati, E.; Giannini, U.; Morini, G.; Galimberti, M.; Barino, L.; Scordamaglia, R. Recent Advances in Propylene Polymerization with $MgCl_2$ Supported Catalysts. *Macromol. Symp.* **1995**, *89*, 73−89.
(18) Scordamaglia, R.; Barino, L. Theoretical Predictive Evaluation of New Donor Classes in Ziegler−Natta Heterogeneous Catalysis for Propene Isospecific Polymerization. *Macromol. Theory Simul.* **1998**, *7*, 399−405.
(19) Toto, M.; Morini, G.; Guerra, G.; Corradini, P.; Cavallo, L. Influence of 1,3-Diethers on the Stereospecificity of Propene Polymerization by Supported Ziegler−Natta Catalysts. A theoretical Investigation on their Adsorption on (110) and (100) Lateral Cuts of MgC_2 Platelets. *Macromolecules* **2000**, *33*, 1134−1140.
(20) Busico, V.; Cipullo, R.; Monaco, G.; Talarico, G.; Vacatello, M.; Chadwick, J. C.; Segre, A. L.; Sudmeijer, O. High-Resolution ^{13}C NMR Configurational Analysis of Polypropylene Made with $MgCl_2$-Supported Ziegler−Natta Catalysts. 1. The "Model" System $MgCl_2$/$TiCl_4$-2,6-Dimethylpyridine/$Al(C_2H_5)_3$. *Macromolecules* **1999**, *32*, 4173−4182.
(21) Taniike, T.; Terano, M. Coadsorption Model for First-Principle Description of Roles of Donors in Heterogeneous Ziegler−Natta Propylene Polymerization. *J. Catal.* **2012**, *293*, 39−50.
(22) Brambilla, L.; Zerbi, G.; Piemontesi, F.; Nascetti, S.; Morini, G. Structure of $MgCl_2$−$TiCl_4$ Complex in Co-Milled Ziegler−Natta Catalyst Precursors with Different $TiCl_4$ Content: Experimental and Theoretical Vibrational Spectra. *J. Mol. Catal., A* **2007**, *263*, 103−111.
(23) Brambilla, L.; Zerbi, G.; Piemontesi, F.; Nascetti, S.; Morini, F. Structure of Donor Molecule 9,9-Bis(methoxymethyl)-fluorene in Ziegler−Natta Catalyst by Infrared Spectroscopy and Quantum Chemical Calculation. *J. Phys. Chem. C* **2010**, *114*, 11475−11484.
(24) Morini, G.; Albizzati, E.; Balbontin, G.; Mingozzi, I.; Sacchi, M. C.; Forlini, F.; Tritto, I. Microstructure Distribution of Polypropylenes Obtained in the Presence of Traditional Phthalate/Silane and Novel Diether Donors: A Tool for Understanding the Role of Electron Donors in $MgCl_2$-Supported Ziegler−Natta Catalysts. *Macromolecules* **1996**, *29*, 5770−5776.
(25) Credendino, R.; Busico, V.; Causà, M.; Barone, V.; Budzelaar, P. H. M.; Zicovich-Wilson, C. Periodic DFT Modeling of Bulk and Surface Properties of $MgCl_2$. *Phys. Chem. Chem. Phys.* **2009**, *11*, 6525−6532.
(26) Andoni, A.; Chadwick, J. C.; Niemantsverdriet, H. J. W.; Thüne, P. C. The Role of Electron Donors on Lateral Surfaces of $MgCl_2$-Supported Ziegler−Natta Catalysts: Observation by AFM and SEM. *J. Catal.* **2008**, *257*, 81−86.
(27) Cheruvathur, A. V.; Langner, E. H. G.; Niemantsverdriet, J. W. H.; Thüne, P. C. In Situ ATR-FTIR Studies on $MgCl_2$−Diisobutyl Phthalate Interactions in Thin Film Ziegler−Natta Catalysts. *Langmuir* **2012**, *28*, 2643−2651.
(28) Credendino, R.; Pater, J. T. M.; Correa, A.; Morini, G.; Cavallo, L. Thermodynamics of Formation of Uncovered and Dimethyl Ether-Covered $MgCl_2$ Crystallites. Consequences in the Structure of Ziegler−Natta Heterogeneous Catalysts. *J. Phys. Chem. C* **2011**, *115*, 13322−13328.
(29) Correa, A.; Credendino, R.; Pater, J. T. M.; Morini, G.; Cavallo, L. Theoretical Investigation of Active Sites at the Corners of $MgCl_2$ Crystallites in Supported Ziegler−Natta Catalysts. *Macromolecules* **2012**, *45*, 3695−3701.
(30) See, e.g., Correa, A.; Piemontesi, F.; Morini, G.; Cavallo, L. Key Elements in the Structure and Function Relationship of the $MgCl_2$/$TiCl_4$/Lewis Base Ziegler−Natta Catalytic System. *Macromolecules* **2007**, *40*, 9181−9189 and references therein.
(31) Dovesi, R.; Saunders, V. R.; Orlando, R.; Zicovich-Wilson, C. M.; Pascale, F.; Civalleri, B.; Doll, K.; Bush, I. J.; D'Arco, P.; Lunell, M. *Crystal 2009 User Manual*; Turin University: Turin, Italy.
(32) Becke, A. D. Density-Functional Thermochemistry. III. The Role of Exact Exchange. *J. Chem. Phys.* **1993**, *98*, 5648−5652.
(33) Grimme, S. Semiempirical GGA-Type Density Functional Constructed with a Long-Range Dispersion Correction. *J. Comput. Chem.* **2006**, *27*, 1787−1799.
(34) Civalleri, B.; Zicovich-Wilson, C. M.; Valenzano, L.; Ugliengo, P. B3LYP Augmented with an Empirical Dispersion Term as Applied to Molecular Crystals. *CrystEngComm* **2008**, *10*, 405.
(35) Schäfer, A.; Horn, H.; Ahlrichs, R. Fully Optimized Contracted Gaussian Basis Sets for Atoms Lithium to Krypton. *J. Chem. Phys.* **1992**, *97*, 2571−2577.
(36) Boys, S. F.; Bernardi, F. The Calculation of Small Molecular Interactions by the Differences of Separate Total Energies. Some Procedures with Reduced Errors. *Mol. Phys.* **1970**, *19*, 553−566.
(37) Pascale, F.; Zicovich-Wilson, C. M.; Gejo, F. L.; Civalleri, B.; Orlando, R.; Dovesi, R. The Calculation of the Vibrational Frequencies of Crystalline Compounds and Its Implementation in the CRYSTAL Code. *J. Comput. Chem.* **2004**, *25*, 888−897.
(38) Zicovich-Wilson, C. M.; Pascale, F.; Roetti, C.; Saunders, V. R.; Orlando, R.; Dovesi, R. Calculation of the Vibration Frequencies of α-Quartz: The Effect of Hamiltonian and Basis Set. *J. Comput. Chem.* **2004**, *25*, 1873−1881.
(39) Pascale, F.; Zicovich-Wilson, C. M.; Orlando, R.; Roetti, C.; Ugliengo, P.; Dovesi, R. Vibration Frequencies of $Mg_3Al_2Si_3O_{12}$ Pyrope. An ab Initio Study with the CRYSTAL Code. *J. Phys. Chem. B* **2005**, *109*, 6146−6152.
(40) Zhang, I. Y.; Wu, J.; Xu, X. Extending the Reliability and Applicability of B3LYP. *Chem. Commun.* **2010**, *46*, 3057−3070.
(41) Giunchi, G.; Allegra, G. Structural Disorder in Microcrystalline Magnesium Chloride. *J. Appl. Crystallogr.* **1984**, *17*, 172−178.
(42) Sozzani, P.; Bracco, S.; Comotti, A.; Simonutti, R.; Camurati, I. Stoichiometric Compounds of Magnesium Dichloride with Ethanol for the Supported Ziegler−Natta Catalysis: First Recognition and Multidimensional MAS NMR Study. *J. Am. Chem. Soc.* **2003**, *125*, 12881−12893.
(43) Malizia, F.; Fait, A.; Cruciani, G. Crystal Structures of Ziegler−Natta Catalyst Supports. *Chem.—Eur. J.* **2011**, *17*, 13892−13897.
(44) Raucoules, R.; de Bruin, T.; Raybaud, P.; Adamo, C. Theoretical Unraveling of Selective 1-Butene Oligomerization Catalyzed by Iron-bis(arylimino)pyridine. *Organometallics* **2009**, *28*, 5358−5367.
(45) Tobisch, S.; Ziegler, T. Catalytic Oligomerization of Ethylene to Higher Linear α-Olefins Promoted by the Cationic Group 4 [(η_5-Cp-(CMe_2-bridge)-Ph)MII(ethylene)$_2$]+ (M = Ti, Zr, Hf) Active Catalysts: A Density Functional Investigation of the Influence of the

Metal on the Catalytic Activity and Selectivity. *J. Am. Chem. Soc.* **2004**, *126*, 9059−9071.
(46) Credendino, R.; Pater, J. T. M.; Liguori, D.; Morini, G.; Cavallo, L. Investigating Alkoxysilane Coverage and Dynamics on the (104) and (110) Surfaces of $MgCl_2$-Supported Ziegler−Natta Catalysts. *J. Phys. Chem. C* **2012**, *116*, 22980−22986.
(47) Stukalov, D. V.; Zakharov, V. A.; Potapov, A. G.; Bukatov, G. D. Supported Ziegler−Natta Catalysts for Propylene Polymerization. Study of Surface Species Formed at Interaction of Electron Donors and $TiCl_4$ with Activated $MgCl_2$. *J. Catal.* **2009**, *266*, 39−49.